ISSN 1063-7834, Physics of the Solid State, 2015, Vol. 57, No. 11, pp. 2246–2251. © Pleiades Publishing, Ltd., 2015.
Original Russian Text © A.G. Razumnaya, Yu.I. Golovko, N.V. Lyanguzov, Yu.I. Yuzyuk, V.B. Shirokov, V.M. Mukhortov, M. El Marssi, 2015, published in Fizika Tverdogo Tela, 2015, Vol. 57, No. 11, pp. 2181–2185.

FERROELECTRICITY

Ferroelectric Superlattice Based on Barium–Strontium Titanate Solid Solutions

A. G. Razumnaya[a, b], Yu. I. Golovko[c], N. V. Lyanguzov[a], Yu. I. Yuzyuk[a,*], V. B. Shirokov[a, c], V. M. Mukhortov[a, c], and M. El Marssi[b]

[a] *Southern Federal University, ul. Bolshaya Sadovaya 105/42, Rostov-on-Don, 344006 Russia*
[b] *Laboratoire de Physique de la Matière Condensèe (LPMC), Universitéde Picardie Jules Verne, 33 rue Saint Leu, Amiens, 80039 France*
[c] *Southern Scientific Center of the Russian Academy of Sciences, pr. Chekhova 41, Rostov-on-Don, 344006 Russia*
** e-mail: yuzyuk@rambler.ru*

Received May 25, 2015

Abstract—A superlattice of the composition $Ba_{0.8}Sr_{0.2}TiO_3/Ba_{0.4}Sr_{0.6}TiO_3$ has been grown by rf cathode sputtering on a MgO(001) substrate. The unit cell parameters of the superlattice layers along the normal to the substrate, modulation period, and orientation relationships between the film and the substrate have been determined using X-ray diffraction. Based on the temperature dependences of the polarized Raman spectra, it has been revealed that the frequency of soft mode E(TO) increases from 79 to 97 cm^{-1} in the temperature range of 80–350 K. It has been found that there are no characteristic indications of a sequence of phase transitions, which take place in bulk samples of barium–strontium titanate solid solutions of identical compositions, and the transition from the ferroelectric to paraelectric phase in the superlattice occurs at a temperature of ~350 K.

DOI: 10.1134/S1063783415110281

1. INTRODUCTION

Ferroelectric superlattices consisting of several alternating layers can exhibit better functional parameters than those of one-component films or have new properties which are not observed in individual layers. In recent years, ferroelectric superlattices with different combinations of oxide materials have been studied experimentally and theoretically [1–14]. Of particular interest are superlattices based on classical $BaTiO_3$ ferroelectric, because it has unique electrical and optical characteristics promising for their applications in devices of functional electronics [15]. The superlattice properties can be controlled by alternating layers with different chemical compositions and thicknesses, thus varying residual stresses induced by mismatch between the crystal lattices in the adjacent layers. High mechanical stresses and, hence, significant forced strains can bring about the formation of principally new phase states in ferroelectric superlattices, affect spontaneous polarization and permittivity, as well as substantially change the Curie temperature [10, 16].

Distortions of a crystal lattice appeared during the displacement of ions lead not only to changes in the structural parameters determined by X-ray diffraction but also to changes in the phonon spectrum of a crystal. Some lattice vibrations, in particular, the ferroelectric soft mode observed in the Raman spectra, are usually very sensitive to displacements of ions, which cause a change in the structure during the phase transition. The study of the behavior of soft modes is the main source of information on microscopic mechanisms of phase transitions in ferroelectrics, and the frequency of the soft mode is related to the static permittivity.

In this work, the $Ba_{0.8}Sr_{0.2}TiO_3/Ba_{0.4}Sr_{0.6}TiO_3$ (BST-0.8/BST-0.4) superlattice grown on a MgO(001) single-crystal substrate has been studied using X-ray diffraction and Raman spectroscopy with the aim of determining specific features of its structure and the lattice dynamics. The analysis of the temperature dependence of the Raman spectra of the superlattice revealed that the temperature behavior of the ferroelectric soft mode agrees well with the data of measurements of the permittivity in the temperature range of 80–350 K.

2. SAMPLE PREPARATION AND EXPERIMENTAL TECHNIQUE

The multilayer heterostructure consisting of eleven alternating pairs of BST-0.8/BST-0.4 layers on a MgO(001) single-crystal substrate was fabricated

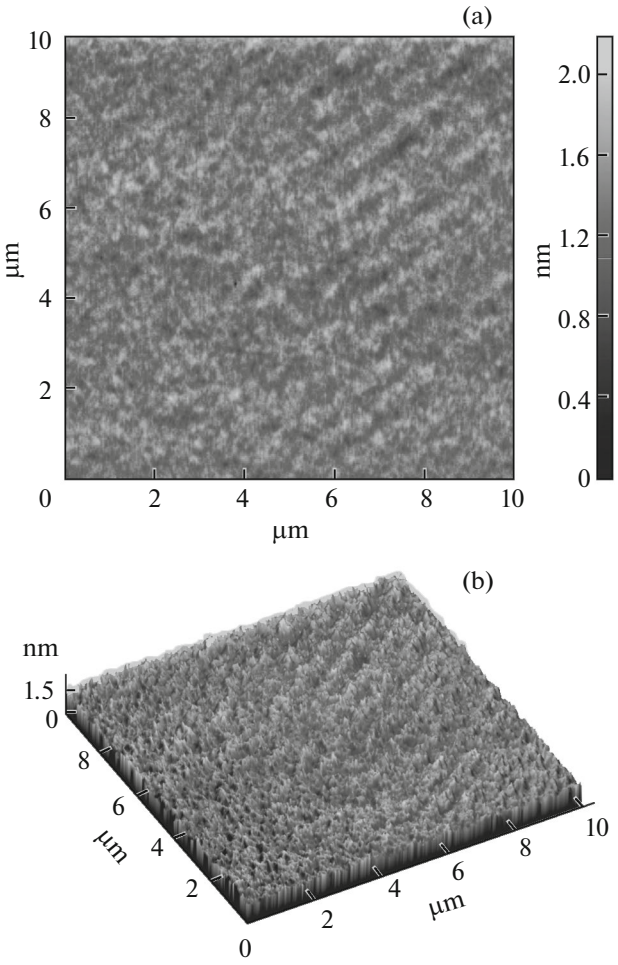

Fig. 1. Microrelief of a surface fragment of the BST-0.8/BST-0.4 heterostructure: (a) two-dimensional image and (b) three-dimensional image.

using two "Plasma 50 SE" rf spattering systems; the targets were stoichiometric ceramic disks 50 mm in diameter. The main difference between this sputtering technique and the known analogs is the use of a high-current rf discharge. Earlier, the rf-sputtering technique was successfully used to prepare epitaxial barium–strontium titanate films [15]. The optimal substrate temperature during deposition of BST-x in a single-crystal state was 870 K. The thicknesses of the BST-0.8 and BST-0.4 layers were obtained using the deposition rate and were ~5 nm; the total thickness of the heterostructure was 110 nm. For a comparative analysis, the BST-0.8 and BST-0.4 films were grown under the same conditions.

The structural perfection of the films, unit cell parameters in the direction of the normal to the substrate plane, and orientational relationships between the film and the substrate at room temperature were found using X-ray diffraction on a DRON-4 diffractometer (CuK_α radiation). The reflections were measured in the θ–2θ scan mode at a scan step of 0.04°C. No impurity phases were observed. The error in the determination of the perovskite unit cell parameters was ±0.0001 nm.

The surface microstructure of the BST-0.8/BST-0.4 heterostructure was studied using an Integra atomic force microscope. The measurements were performed in a semicontact mode using an NSG11 standard silicon cantilever. Figures 1a and 1b show the images of the microrelief of a 10 × 10 μm surface fragment of the heterostructure. The analysis of the morphology showed that the average roughness of the film is only 0.13 nm, and the maximum height of the surface relief is less than 2 nm.

For dielectric measurements, the planar topology of electrodes based on a vanadium sublayer (20 nm) and an aluminum electrode (2 μm) was formed as an interdigitated system. The widths of the metallic strips and the gaps between them were 2 μm, and the total width of 78 strips with gaps between them was 318 μm. The interdigitated system was formed by explosive photolithography. The capacity, conductivity, and leakage currents of the planar capacitors were measured using a Keihtley 4200SCS multimeter at a frequency of 1 MHz with a PM-5 MicroTec probe station. The dielectric loss tangent was no higher than 0.0014, and the leakage currents of the planar capacitor were less than 10^{-10} A.

The Raman spectra were excited by polarized radiation from an argon laser (λ = 514.5 nm) and were measured using a Renishaw one-pass spectrometer equipped with a Near-Excitation Tuneable (NExT) filter for analysis of low-frequency spectral regions. The exciting radiation was focused on the sample using a Leica optical microscope; the focused beam diameter on the sample was 2 μm. The polarized Raman spectra were measured on the samples which were exactly oriented in correspondence with the crystallographic axes of the substrates: $X \parallel$ [100]MgO, $Y \parallel$ [010]MgO, and $Z \parallel$ [001] MgO. The spectra of the BST-0.8/BST-0.4 heterostructure were measured in the side-view backscattering geometry [17], when the wave vector of the incident beam was parallel to the substrate, while the polarization of the incident and scattered light beams were parallel or perpendicular to the Z axis of the film. The intensities of all the spectrograms were corrected for the temperature factor.

3. RESULTS AND DISCUSSION

The X-ray diffraction pattern of the multilayer BST-0.8/BST-0.4 heterostructure measured in the θ–2θ scan mode contains only reflections (00l) from the BST-0.8/BST-0.4 heterostructure and reflections (002) and (004) from the MgO substrate, which demonstrates the parallel orientation of the heterostructure layer with respect to the MgO(001) substrate. The vertical misorientation relative to the normal to the substrate found from the widths of curves of

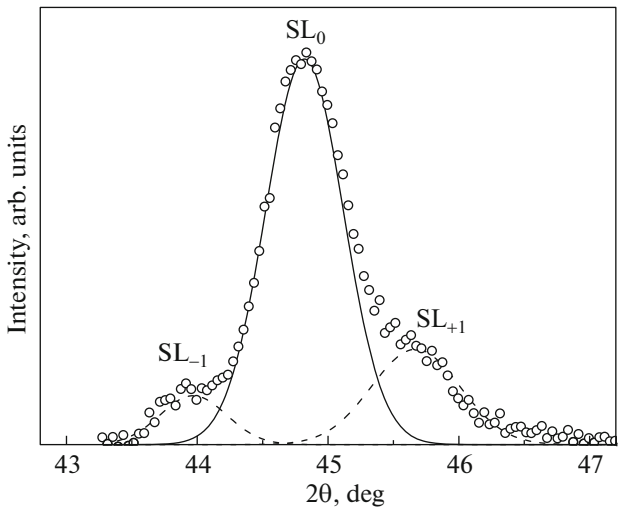

Fig. 2. Fragment of the X-ray diffraction pattern with the profile of the (002) reflection of the multilayer BST-0.8/BST-0.4 heterostructure and the decomposition of this profile into components.

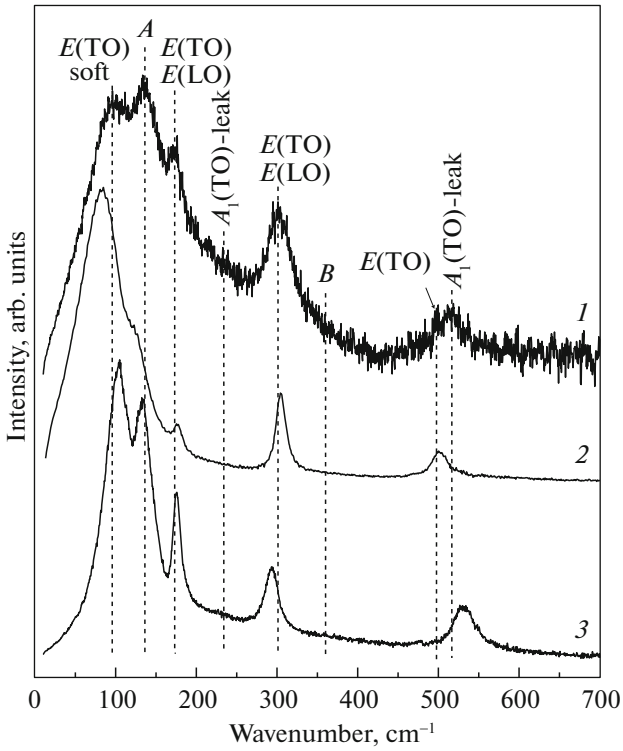

Fig. 3. Polarized Raman spectra of (*1*) the BST-0.8/BST-0.4 superlattice, (*2*) BST-0.8 film, and (*3*) BST-0.4 film measured in the scattering geometry $Y(XZ)\bar{Y}$ at room temperature.

reflection (002) is ~2°. Figure 2 shows a fragment of X-ray diffraction pattern near reflection (002) of the BST-0.8/BST-0.4 heterostructure measured by the θ–2θ scanning method.

A specific feature of reflection (002) is that it is substantially spread and asymmetric. The experimental profile cannot be interpreted as a superposition of reflections of two independent BST-0.8 and BST-0.4 layers. The analysis of the shape of the experimental profile of symmetric reflection (002) makes it possible to conclude that it can be represented as main peak SL_0 and two neighboring satellites SL_{-1} and SL_{+1} (Fig. 2). This fact demonstrates that the structure exhibits a periodicity that is characteristic of the superlattices.

The modulation period Λ was obtained from the angular positions of the satellites in the reflection [18]

$$\Lambda = \lambda/(2(\sin\theta_{n+1} - \sin\theta_n)),$$

where λ is the X-ray radiation wavelength, θ_{n+1} and θ_n are the angular positions of the neighboring maxima in the reflection, and n is the reflection order with respect to the modulation period Λ. The modulation period of the superlattice is $\Lambda = L_{\text{BST-0.8}} + L_{\text{BST-0.4}}$, where $L_{\text{BST-0.8}}$ is the thickness of the BST-0.8 layer and $L_{\text{BST-0.4}}$ is the thickness of the BST-0.4 layer. Thus, based on the X-ray diffraction data, it was found that modulation period Λ of the BST-0.8/BST-0.4 superlattice is 11.2 nm with the layer thicknesses $L_{\text{BST-0.8}}$ = 5.4 nm and $L_{\text{BST-0.4}}$ = 5.8 nm.

The unit cell parameters c of the superlattice layers were determined by fitting of the calculated reflection profiles to the experimental profiles. The calculations were carried out in terms of the kinematic theory of X-ray scattering as described in [19]. The fitting process was accompanied by varying the number of unit cells in the layers and the unit cell parameters of the layers. We did not take into account the thickness of the interface between the layers and assumed that the thickness of each of the layers is constant.

As a result of the processing of the diffraction profile of the superlattice, it was found that the unit cell parameters c of the BST-0.8 and BST-0.4 layers are larger than those in the bulk materials and are 0.4047 and 0.4035 nm, respectively. In the BST-0.8 solid solution, the unit cell parameters are c = 0.3991 nm and a = 0.3978 nm, and the BST-0.4 composition is cubic at room temperature with the lattice parameter a = 0.3929 nm. The increase in parameters c of the BST-0.8 and BST-0.4 layers as compared to those of the bulk free materials can be due to the compression in the conjugation plane. Thus, we can suggest that the BST-0.8 and BST-0.4 layers are distorted tetragonally.

Figure 3 shows the Raman spectra of the BST-0.8/BST-0.4 superlattice and the BST-0.8 and BST-0.4 films measured at room temperature in the scattering geometry $Y(XZ)\bar{Y}$ corresponding to the E-type modes, assuming the tetragonal symmetry [17]. Because the E(TO) component of the soft mode corresponds to the displacement of Ti ions with respect to

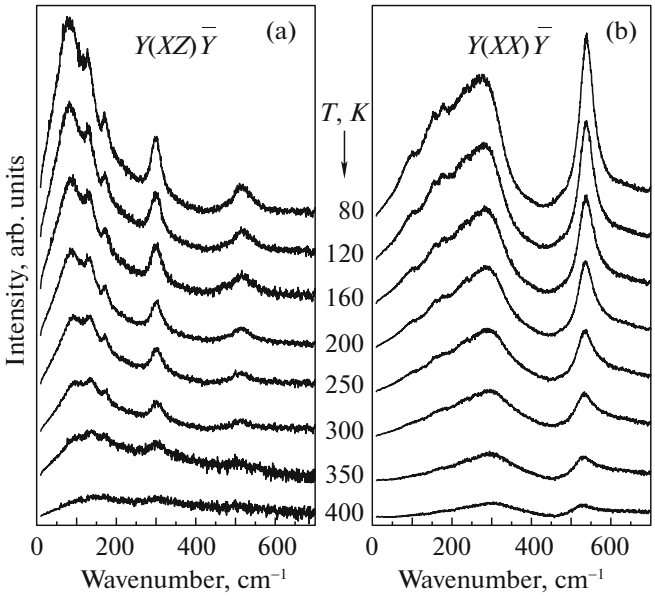

Fig. 4. Polarized Raman spectra of the BST-0.8/BST-0.4 superlattice measured in the scattering geometries (a) $Y(XZ)\bar{Y}$ and (b) $Y(XX)\bar{Y}$ at room temperature.

the oxygen octahedron in the plane parallel to the substrate, its frequency is sensitive to the value of the two-dimensional clamping in the heterostructure. In the BST-0.8 film, the frequency of the soft mode E(TO) is 81 cm^{-1}, and its half-width is 66 cm^{-1}. In the BST-0.4 film, the frequency of the soft mode E(TO) at room temperature is significantly higher (103 cm^{-1}), and its half-width is 41 cm^{-1}. In the superlattice consisting of alternating BST-0.8 and BST-0.4 layers, the frequency of the soft mode E(TO) is 95 cm^{-1}, and its half-width is 84 cm^{-1}. As seen from Fig. 3, all phonon modes of the Raman spectra of the BST-0.8 and BST-0.4 films and the BST-0.8/BST-0.4 superlattice demonstrate a similar behavior. Thus, in the scattering geometry $Y(XZ)\bar{Y}$, the Raman spectrum of the BST-0.8/BST-0.4 superlattice can be interpreted as a superposition of the spectra of the BST-0.8 and BST-0.4 films.

Figures 4a and 4b show the temperature dependences of the polarized Raman spectra of the BST-0.8/BST-0.4 superlattice measured in the frequency range $10 < \nu < 700$ cm^{-1} in the scattering geometries $Y(XZ)\bar{Y}$ and $Y(XX)\bar{Y}$. The Raman spectra of the tetragonal ferroelectric phase measured in the diagonal scattering geometry $Y(XX)\bar{Y}$ contain the longitudinal (LO) and transverse (TO) optical modes of symmetry A_1, mode B_1, and the contribution from the mode E(TO) at low frequencies (80–90 cm^{-1}) due to the non-diagonal scattering geometry $Y(XZ)\bar{Y}$. The spectra measured in the scattering geometry $Y(XZ)\bar{Y}$ contain modes E(TO) and E(LO), as well as an insignificant contribution of the A_1-type lines (270 and 535 cm^{-1}) penetrating from the diagonal scattering geometries.

As is known [20], the spectrum of the paraelectric phase of $BaTiO_3$ crystal with symmetry O_h^1 has two broad bands at frequencies near 260 and 530 cm^{-1} induced by a disorder, although all optical modes are forbidden in Raman spectra. As temperature decreases, narrow lines of polar modes arise against the background of these broad bands having a complex structure upon the transition from the paraelectric to the tetragonal ferroelectric phase. Similar temperature behavior of phonon modes in the Raman spectrum is also observed in the superlattice under study below 350 K. From Fig. 4, we can see that, as temperature increases, all changes in the spectra occur smoothly, but the intensity of polar modes increases monotonically as temperature decreases. Note that we did not observe specific features of the phase transitions which take place in bulk samples of the BST-0.8 and BST-0.4 solid solutions. It is seen from the temperature dependences of the spectra measured in the scattering geometry $Y(XX)\bar{Y}$ that the frequencies of the A_1 modes are not markedly changed in the temperature range of 80–350 K (Fig. 4b). Based on the analysis of the temperature dependence of the phonon mode frequencies measured in the scattering geometry $Y(XZ)\bar{Y}$, it can be noted that the frequencies of the E(TO)-type polar modes observed in the spectra of the BST-0.8/BST-0.4 heterostructure are weakly dependent on temperature. Their intensities gradually decrease and their half-widths increase with temperature (Fig. 4a). Unlike other phonon modes, the E(TO) component of the soft mode demonstrates a significant temperature dependence (Fig. 5a); however, sharp jumps of the parameters of the soft mode components are not observed as temperature increases from 80 to 350 K. In the BST-0.8/BST-0.4 superlattice, the frequency of the soft mode E(TO) is 79 cm^{-1} at 80 K and monotonically increases with temperature to 97 cm^{-1} at 350 K; simultaneously, its half-width increases from 81 to 85 cm^{-1}. Based on the extrapolation of the temperature dependence of the integrated intensity of the soft mode E(TO), it can be suggested that the superlattice undergoes the transition to the paraelectric phase at a temperature of ~350 K.

In the tetragonal phase, the permittivity in the substrate plane ε_1 is determined by phonons of the E symmetry, while permittivity $\varepsilon_\parallel$ is determined by phonons of the A_1 symmetry [20]. The dominant contribution to $\varepsilon_\perp$ is due to frequency ν of transverse soft mode E(TO), so that $\varepsilon_\perp \sim 1/\nu^2$. Figure 5b shows the temperature dependences of the normalized capacitance of the BST-0.8/BST-0.4 superlattice measured in the substrate plane and $1/\nu^2$ of the soft mode E(TO). It can be seen that the capacitance that is proportional to permittivity $\varepsilon_\perp$ decreases monotonically as tempera-

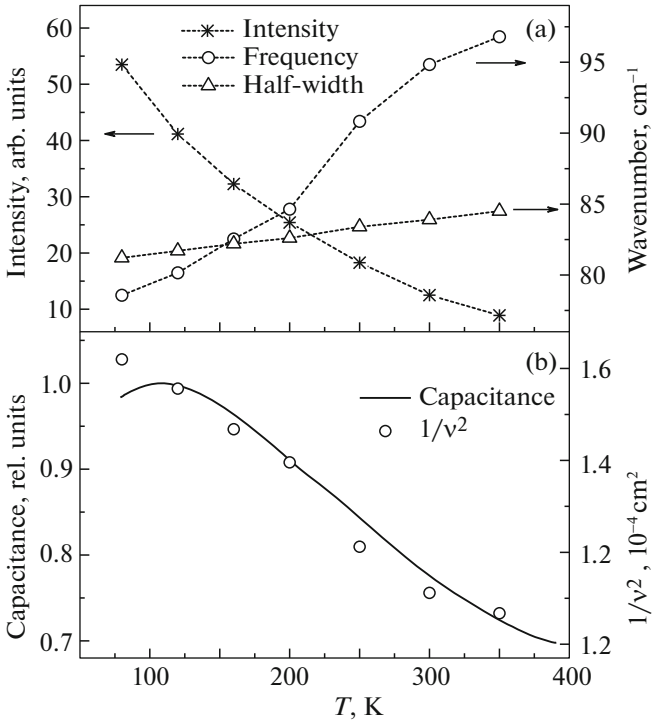

Fig. 5. (a) Temperature dependences of (a) the integrated intensity, frequency, and half-width of the soft mode E(TO) of the BST-0.8/BST-0.4 superlattice and (b) temperature dependences of the normalized capacitance (solid line) and $1/\nu^2$ of the soft mode E(TO) (points) of the BTS-0.8/BST-0.4 superlattice..

ture increases to 400 K. Quantity $1/\nu^2$ of the soft mode E(TO) behaves similarly in the temperature range of 80–350 K (Fig. 5b). Thus, we can conclude that the behavior of low-frequency transverse soft mode E(TO) determines the monotonic temperature dependence of the static permittivity of the superlattice under study.

4. CONCLUSIONS

The BST-0.8/BST-0.4 superlattice with tetragonally distorted nanolayers was synthesized by rf cathode sputtering. The atomic force microscopy study of the surface morphology of this superlattice showed that the surface is specularly smooth with the average roughness of 0.13 nm, which makes it possible to integrate heterostructures of this type in devices of microsystem and microwave engineering as a base element. Based on the X-ray diffraction data, we found that the film and the substrate orientations are completely parallel to each other. Moreover, we determined the unit cell parameters of the superlattice layers and the superlattice modulation period equal to 11.2 nm, which agrees well with the period calculated from the deposition rate of the layers. We studied the temperature dependences of the polarized Raman spectra of the BST-0.8/BST-0.4 superlattice and did not find indications of phase transitions that occur in bulk samples of BST solid solutions of the same compositions. Based on the temperature dependence of the Raman spectra, it was found that the transition from the ferroelectric to paraelectric phase is observed in the superlattice at a temperature of ~350 K. The analysis of the Raman spectra showed that the frequency of the soft mode E(TO) increases from 79 to 97 cm^{-1} as the temperature increases from 80 to 350 K. It was found that the change in the static permittivity correlates with the change in the frequency of the soft mode E(TO).

ACKNOWLEDGMENTS

The authors are grateful to the European Research Net FP7-ITN for the possibility of scientific exchange on the ITN–NOTEDEV program.

This study was supported by the Russian Foundation for Basic Research (project no. 14-12-00258).

REFERENCES

1. H. Tabata, H. Tanaka, and T. Kawai, Appl. Phys. Lett. **65**, 1970 (1994).
2. O. Diéguez, S. Tinte, A. Antons, C. Bungaro, J. B. Neaton, K. M. Rabe, and D. Vanderbilt, Phys. Rev. B: Condens. Matter **69**, 212101 (2004).
3. S. Lisenkov and L. Bellaiche, Phys. Rev. B: Condens. Matter **76**, 020102(R) (2007).
4. N. Ortega, A. Kumar, O. A. Maslova, Yu. I. Yuzyuk, J. F. Scott, and R. S. Katiyar, Phys. Rev. B: Condens. Matter **83**, 144108 (2011).
5. S. Rios, J. F. Scott, A. Lookman, J. McAneney, R. M. Bowman, and J. M. Gregg, J. Appl. Phys. **99**, 024107 (2006).
6. M. El Marssi, Y. Gagou, J. Belhadi, F. DeGuerville, Yu. I. Yuzyuk, and I. P. Raevski, J. Appl. Phys. **108**, 084104 (2010).
7. O. A. Maslova, Yu. I. Yuzyuk, N. Ortega, A. Kumar, and R. S. Katiyar, Phys. Solid State **53** (5), 1062 (2011).
8. A. I. Lebedev, J. Adv. Dielectr. **2**, 1250003 (2012).
9. A. S. Anokhin, O. A. Bunina, Yu. I. Golovko, V. M. Mukhortov, Yu. I. Yuzyuk, and P. Simon, Thin Solid Films **545**, 267 (2013).
10. N. Ortega, A. Kumar, O. Resto, O. A. Maslova, Yu. I. Yuzyuk, J. F. Scott, and R. S. Katiyar, J. Appl. Phys. **114**, 104102 (2013).
11. Yu. A. Tikhonov, A. G. Razumnaya, O. A. Maslova, I. N. Zakharchenko, Yu. I. Yuzyuk, N. Ortega, A. Kumar, and R. S. Katiyar, Phys. Solid State **57** (3), 486 (2015).
12. Yu. A. Tikhonov, I. N. Zakharchenko, O. A. Maslova, Yu. I. Yuzyuk, N. Ortega, A. Kumar, and R. S. Katiyar, Phys. Solid State **56** (3), 594 (2014).
13. J. Belhadi, M. El Marssi, Y. Gagou, Yu. I. Yuzyuk, Y. El Mendili, I. P. Raevski, H. Bouyanfif, and J. Wolfman, J. Appl. Phys. **116**, 034108 (2014).

14. Yu. A. Tikhonov, A. G. Razumnaya, V. I. Torgashev, I. N. Zakharchenko, Yu. I. Yuzyuk, M. El Marssi, N. Ortega, A. Kumar, and R. S. Katiyar, Phys. Status Solidi RRL **9**, 68 (2015).
15. V. M. Mukhortov and Yu. I. Yuzyuk, *Heterostructures Based on Nanoscale Ferroelectric Films: Preparation, Properties, and Applications* (Southern Scientific Center of the Russian Academy of Sciences, Rostov-on-Don, 2008) [in Russian].
16. V. B. Shirokov, Yu. I. Golovko, V. M. Mukhortov, Yu. I. Yuzyuk, P. E. Janolin, and B. Dkhil, Phys. Solid State **57** (8), 1529 (2015).
17. Yu. I. Yuzyuk, Phys. Solid State **54** (5), 1026 (2012).
18. F. Le Marrec, R. Farhi, M. El Marssi, J. L. Dellis, M. G. Karkut, and D. Ariosa, Phys. Rev. B: Condens. Matter **61**, R6447 (2000).
19. I. K. Schuller, Phys. Rev. Lett. **44**, 1597 (1980).
20. A. Scalabrin, A. S. Chaves, D. S. Shim, and P. S. Porto, Phys. Status Solidi B **79**, 731 (1977).

Translated by Yu. Ryzhkov